Eur. Phys. J. A **27**, 167–181 (2006)
DOI 10.1140/epja/i2005-10253-5

THE EUROPEAN PHYSICAL JOURNAL A

Alpha-induced fragmentation of ^{28}Si in a statistical model

M.S. Sabra[1,a], Z.F. Shehadeh[2,3], and F. Bary Malik[1,4]

[1] Physics Department, Southern Illinois University, Carbondale, IL 62901, USA
[2] Applied Science University, Amman, Jordan
[3] Taif Teachers College, Taif, Saudi Arabia
[4] Physics Department, Washington University, St. Louis, MO 63130, USA

Received: 24 June 2005 / Revised version: 8 February 2006 /
Published online: 30 March 2006 –
Communicated by C. Signorini

Abstract. Within the context of a statistical model, that incorporates final-state interaction between a pair of fragments, we have calculated the energy spectra associated with the production of different isobaric pairs as a function of their lab kinetic energy and isobaric and elemental distributions of nuclei produced in the ^{4}He + ^{28}Si reaction at cm incident energies of 102.7, 173.7, 300, 500, and 1000 MeV. Double differential cross-section of isobars 16, 20, and 24 as a function of their lab kinetic energies at 30° and the same for isobar 24 at 10°, 30°, 60°, and 90° have been calculated at cm incident energies of 102.7 and 173.7 MeV and compared with the data of Woo *et al.* Calculated yields follow the trend of the data at each angle, and calculated angular distributions also reproduce the general trend of the observed ones. A key feature of the model is that it allows for fragments to be emitted in ground states as well as in excited states that are allowed by the conservation of energy. The analysis establishes that the fragments are emitted in excited state. The excitation energies for $A = 24$ and 16 are deduced from the data. The observed angular distributions for $A = 7$, 12, 16, 20, 24, and 28 are well accounted for assuming them to be emitted in excited states. The relative production probabilities for different elements and isobars are energy dependent. The yields for unstable elements, ^{5}Li, ^{8}Be, and ^{26}Al, are found to be significant. The relative fragmentation probabilities of all allowed isotopic pairs have been presented.

PACS. 24.60.Dr Statistical compound-nucleus reactions – 25.55.-e ^{3}H-, ^{3}He-, and ^{4}He-induced reactions – 25.60.Gc Breakup and momentum distributions

1 Introduction

Outside the proactive cocoon of the Earth's atmosphere is a universe full of radiation. Space contains elements from hydrogen to nickel in various proportions. These elements collide with the walls of space crafts causing the emission of secondary radiation inside space crafts, which is a serious hazard to occupants as well as instruments in the cabin [1]. The development of protecting devices requires the knowledge of the radiation level inside the cabin caused by secondary radiation that is made of fragmentation of nuclei of the elements of the wall by incident galactic nuclei. Because of the varied nature of galactic nuclei and their broad energy spectra, much of the production cross-sections are to be determined theoretically. Aside from this, micro-electronic measuring devices, containing quite often silicon and oxygen, are, in some cases, directly exposed to galactic nuclear radiation. The subject matter of this topic would provide an understanding of the fragmentation of silicon by alpha-particle, the second most abundant element in space. It is also to be noted that the understanding of this process is also important in determining the elemental distribution in the cosmos [2].

Since any theoretical model to describe fragmentation involves approximations, it is necessary to test the model against existing data. Such data exist for fragmentation of ^{28}Si by 117.4 and 198.5 MeV (lab) alpha-particles. Attempts to understand them within the context of an evaporation model had only a limited success. We, therefore, first try to account for these data theoretically.

Alpha-particles with lab kinetic energies of 117.4 and 198.5 MeV ($E/A \approx 29$ and 50 MeV/nucleon) are close to the energy range used in explaining the fragmentation of ^{16}O by proton using a statistical model [3]. This model distinguishes itself from the direct production models discussed in [1] in at least one important aspect: it includes the possibility that the fragments are being emitted both in ground and in excited states. The method used in [3]

[a] e-mail: sabra@siu.edu

also incorporates final-state interaction between two members of the emerging fragments, which is distinct from the usual evaporation model.

A key assumption of the model is the formation of a compound nucleus (CN) as an intermediate step, which, then, decays to a pair of interacting fragments of varied excitation energies allowed by the law of energy conservation.

Within the framework of this model, we have examined the experimental data of Woo *et al.* [4] on the fragmentation of ^{28}Si by 117.4 and 198.5 MeV (lab) alpha-particles, and find that the overall trend of these data is reasonably accounted for by the calculation. We, therefore, present here the relative probabilities of isobaric and isotopic productions of nuclei from $A = 1$ to 31 in the fragmentation of ^{28}Si by alpha-particle from threshold energy to 1.0 GeV (cm) within the context of this model. At incident energies above that, the treatment would require the inclusion of relativistic effects, which is beyond the scope of this treatment.

In this next section, we present the theory followed by a section on the determination of the final-state interaction used in the calculation. In sect. 4, we discuss the results first for incident alpha-particle energies of 117.4 and 198.5 MeV (lab), and then for 300, 500 and 1000 MeV (cm).

2 Theory

According to the statistical theory of Weisskopf and Ewing [5], Newton [6], and Ericson [7], a nuclear reaction takes place in two steps: a) the incident particle together with the target nucleus form a compound nucleus, CN, and b) the CN then decays to final products. The two steps can be considered as separate processes following one another. The total cross-section of the whole process is, then, basically, the cross-section for the formation of the CN and its subsequent decay probabilities into final products.

In this work, we consider the fragmentation of the CN into a pair of fragments, *i.e.* binary fragmentation, each of which could be in ground and all possible excited states allowed by the energy conservation. The double differential cross-section for the production of a pair of fragments A_1 and A_2 in the final channel α' from the entrance channel α, in the cm system, is given by

$$\frac{\mathrm{d}^2\sigma_{\alpha\alpha'}}{\mathrm{d}\Omega\mathrm{d}\varepsilon} = \sigma_C \left(\frac{P_{\alpha'}\left(I, U_C, \theta, \varepsilon\right)}{\sum\limits_{\alpha'} P_{\alpha'}\left(I, U_C\right)} \right), \tag{1}$$

where σ_C is the formation cross-section of the CN with spin I and excitation energy U_C, $P_{\alpha'}(I, U_C, \theta, \varepsilon)$ is the decay probability of the CN into a pair of fragments A_1 and A_2 with relative energy, ε, in a direction making an angle θ with the incident beam in the final channel α', and $P_{\alpha'}(I, U_C)$ is the decay probability of a particular pair of fragments over all angles with all possible excitation energies allowed by the conservation of energy, and the sum is over all possible final channels α'. Following Ericson [7], the numerator in (1) is given by

$$\begin{aligned} P_{\alpha'}(I, U_C, \theta, \varepsilon) = {} & \frac{1}{\rho_C(I, U_C)} \frac{T_l^{12}(\varepsilon)}{\hbar\sqrt{2\pi^5}} \\ & \times \int_0^{Q_0+T_{cm}-\varepsilon} \frac{(\sigma_1^2\sigma_2^2)^{\frac{3}{2}}}{\sqrt{\sigma_1^2+\sigma_2^2}} \rho_1(j_1, U_1)\rho_2(j_2, U_2) \\ & \times e^{\frac{-I^2\sin^2\theta}{4(\sigma_1^2+\sigma_2^2)}} J_0\left(i\frac{I^2\sin^2\theta}{4\left(\sigma_1^2+\sigma_2^2\right)}\right) \mathrm{d}U_1\,, \end{aligned} \tag{2}$$

where $\rho_C(I, U_C)$ is the level density function of the CN with spin I and excitation energy U_C; $\rho(j_i, U_i)$, and σ_i^2, with $i = 1, 2$, are, respectively, the level density function and the spin-cutoff factor for the two emerging fragments A_1 and A_2; $J_0(x)$ is the modified Bessel function of zeroth order; Q_0 is the total Q-value of the reaction, *i.e.* the energy required for the decay to the ground states of fragments pair, and T_{cm} is the cm incident energy in the entrance channel α. The transmission coefficient in (2), $T_l^{12}(\varepsilon)$, is that between the two emerging fragments in the final channel α'. Following Ericson [7], we replace the transmission coefficient, $T_l^{12}(\varepsilon)$, by its value for $l = 0$, *i.e.* $T_0^{12}(\varepsilon)$, implying that the decay probabilities are dominated by zero orbital angular momentum.

For the level density function $\rho(j, U)$, j and U being the spin and excitation energy of the level, respectively, we have adopted here the expression of Gadioli and Zetta [8] derived by analyzing many experimental data. It is given by

$$\rho(j, U) = \frac{\hbar^3}{12\sqrt{8}}(2j+1)e^{\left(\frac{-j(j+1)}{2\sigma^2}\right)} a^{\frac{1}{2}}\, g^{\frac{-3}{2}}\, \frac{e^{\left(2\sqrt{au}\right)}}{(u+t)^2}\,, \tag{3}$$

where a and g are, respectively, the level density parameter, $0.127A\,\mathrm{MeV}^{-1}$, and the nuclear moment of inertia, $0.7[(2/5)AR^2]$, with A is the mass number of the fragment in consideration, and $R = 1.5A^{1/3}$ fm; σ^2 is the spin-cutoff factor, $(g/\hbar^2)[(u+t)/a]^{1/2}$, where $\hbar$ is Planck's constant h divided by 2π, u is the *effective excitation energy*, $u = U - \Delta + (70/A)$, Δ being the pairing energy [9], and t is the thermodynamics nuclear temperature, $u = at^2 - t$.

The level density formula, (3), is not valid at very low excitation energies. At low energies we have approximated it by applying a cutoff. The cutoff in the level density is taken to be 5 MeV for all fragments except for the proton, neutron and the helium isotopes, for which it is taken to be 50 MeV. Above the cutoff energy, the level density is given by (3) and below the cutoff energy, it is replaced by 1/cutoff.

Since the fragments emerging from the CN are mainly in highly excited states, we cannot determine their spins with any degree of certainty. Fortunately, the level density function represented by (3) is a slowly varying function of spin j, therefore we can use it to determine the level density function of either fragment by setting the value of the spin j to zero, *i.e.* $\rho(j, U) = \pi\,\rho(0, U)$. This can be done without introducing any significant error into our calculations. After this replacement, we obtain the probability of

decay for a CN into a pair of fragments A_1 and A_2 with relative energy ε in a given direction θ to be the following expression:

$$P_{\alpha'}(I,U_C,\theta,\varepsilon) = \frac{\hbar^5}{1152\sqrt{2\pi}} \frac{\sqrt{a_1\, a_2}}{\rho_C(I,U_C)} (g_1\, g_2)^{\frac{-3}{2}} T_0^{12}(\varepsilon) \times \int_0^{Q_0+T_{cm}-\varepsilon} \frac{\left(\sigma_1^2\, \sigma_2^2\right)^{\frac{3}{2}}}{\sqrt{\sigma_1^2+\sigma_2^2}} \frac{e^{(2(\sqrt{a_1 u_1}+\sqrt{a_2 u_2}))}}{(u_1+t_1)^2\,(u_2+t_2)^2} \times e^{\frac{-I^2\sin^2\theta}{4(\sigma_1^2+\sigma_2^2)}} J_0\left(i\frac{I^2\sin^2\theta}{4\,(\sigma_1^2+\sigma_2^2)}\right) \mathrm{d}U_1\,, \quad (4)$$

where $u_1 = U_1 - \Delta_1 + (70/A_1)$ and $u_2 = Q_0 + T_{cm} - \varepsilon - \Delta_2 + (70/A_2) - U_1$.

The differential cross-section, $\mathrm{d}\sigma_{\alpha\alpha'}/\mathrm{d}\Omega$, can be obtained by integrating $P_{\alpha'}(I,U_C,\theta,\varepsilon)$ over all possible values for ε:

$$\frac{\mathrm{d}\sigma_{\alpha\alpha'}}{\mathrm{d}\Omega} = \sigma_C \left(\frac{P_{\alpha'}(I,U_C,\theta)}{\sum\limits_{\alpha'} P_{\alpha'}(I,U_C)}\right), \quad (5)$$

where

$$P_{\alpha'}(I,U_C,\theta) = \int_0^{Q_0+T_{cm}} P_{\alpha'}(I,U_C,\theta,\varepsilon)\,\mathrm{d}\varepsilon. \quad (6)$$

Hence, the total cross-section, $\sigma_{\alpha\alpha'}$, can be obtained by integrating $P_{\alpha'}(I,U_C,\theta)$ over all angles, where the decay probability $P_{\alpha'}(I,U_C)$ of the CN into a pair of fragments over all energies at all angles is given by

$$P_{\alpha'}(I,U_C) = 2\pi \int_0^{\pi} P_{\alpha'}(I,U_C,\theta)\sin\theta\,\mathrm{d}\theta. \quad (7)$$

The transmission coefficient, $T_0^{12}(\varepsilon)$, in (4) can be determined from the solution of the time-independent Schrödinger equation in spherical polar coordinates. In order to obtain $T_0^{12}(\varepsilon)$, one needs knowledge of the nuclear interaction, $V_N(r)$, between the pair of fragments in the final channel α'. For this purpose, we take the potential to be of a complex molecular type because a) the energy-density functional formalism [10–13] as well as the two-centered shell model calculation [14] indicates its real part to be non-monotonic, b) the inverse scattering theory of Alam and Malik [15] for the ^{12}C–^{12}C interaction has determined the potential to be of this type, and c) experimental data can be fitted with this potential [16–18]. Another important advantage of using a complex molecular potential is that one can obtain the potential between two nuclei by a scaling procedure of the parameters determined for a given system [13,17]. This is demonstrated by Haider and Malik [17] who scaled the potential for the ^{12}C–^{12}C system using information obtained from their previous study of the interaction of the ^{16}O–^{16}O system and by Manngard, Brenner, Reichstein and Malik [19], who obtained the α-^{32}S potential by scaling the α-^{28}Si potential, as well as by Shehadeh [20].

In the final channels, there are usually no elastic scattering data to determine the potential. But we have used the scaling procedure suggested by Haider and Malik [17] to determine the complex potential between the pair of fragments for all cases, except for proton and neutron channels, where we have used the optical potential used by Compani-Tabrizi and Malik [3]. Such potentials seem to explain the data for the cases under considerations.

3 The complex molecular potential

The complex molecular potential is the sum of the real and imaginary potentials:

$$V(r) = V_{real}(r) + iV_{imag}(r), \quad (8)$$

where

$$V_{real}(r) = \frac{V_0}{1+e^{\left[\frac{r-R_0}{a_0}\right]}} + V_1 e^{\left[-\left(\frac{r}{R1}\right)^{n_1}\right]} + V_C(r) \quad (9)$$

with the Coulomb potential, $V_C(r)$, being that of a uniformly charged sphere given by

$$V_C(r) = \begin{cases} \frac{Z_1 Z_2 e^2}{2R_C}\left(3-\frac{r^2}{R_C^2}\right), & r \le R_C\,, \\ \frac{Z_1 Z_2 e^2}{r}, & r > R_C\,, \end{cases} \quad (10)$$

where Z_1 and Z_2 are the charges of the fragments pair, and R_C is the Coulomb radius.

The strength of the attractive part V_0 can be scaled as in [17]

$$V_0 = b_s\left(A_1^{\frac{2}{3}} + A_2^{\frac{2}{3}} - (A_1+A_2)^{\frac{2}{3}}\right) \quad (11)$$

with $b_s = -10.2\,\mathrm{MeV}$, and A_1 and A_2 are the mass numbers for the fragments pair. The diffuseness parameter a_0 is about 0.53 fm. The depth of the repulsive part V_1 is 100 MeV.

The imaginary part of the potential, $V_{imag}(r)$, is taken to be of the form

$$V_{imag}(r) = W(\varepsilon)\, e^{\left[-\left(\frac{r}{R_2}\right)^{n_2}\right]}. \quad (12)$$

The coefficient $W(\varepsilon)$ is assumed to have an energy dependence and is determined to be

$$W(\varepsilon) = V_2\left(1 + C_1\varepsilon + C_2\varepsilon^2\right), \quad (13)$$

where ε is the relative energy of the fragments pair. The coefficients V_2, C_1, and C_2 of the imaginary part of the potential have previously been determined by Haider and Malik [17] to be $-1.613\,\mathrm{MeV}$, $0.02\,\mathrm{MeV}^{-1}$ and $0.012\,\mathrm{MeV}^{-2}$, respectively, and n_1 in (9) and n_2 in (12) are taken to be 2.

The radii R_0, R_1, R_2, and R_c can be expressed in the following manner:

$$R_i = r_i\left(A_1^{\frac{1}{3}} + A_2^{\frac{1}{3}}\right), \quad i = 0,1,2,c \quad (14)$$

with $r_0 = r_c = 1.35\,\mathrm{fm}$, $r_1 = 0.52\,\mathrm{fm}$, and $r_2 = 0.83\,\mathrm{fm}$.

Thus, one can obtain the potential between two emerging fragments from their mass and charge numbers.

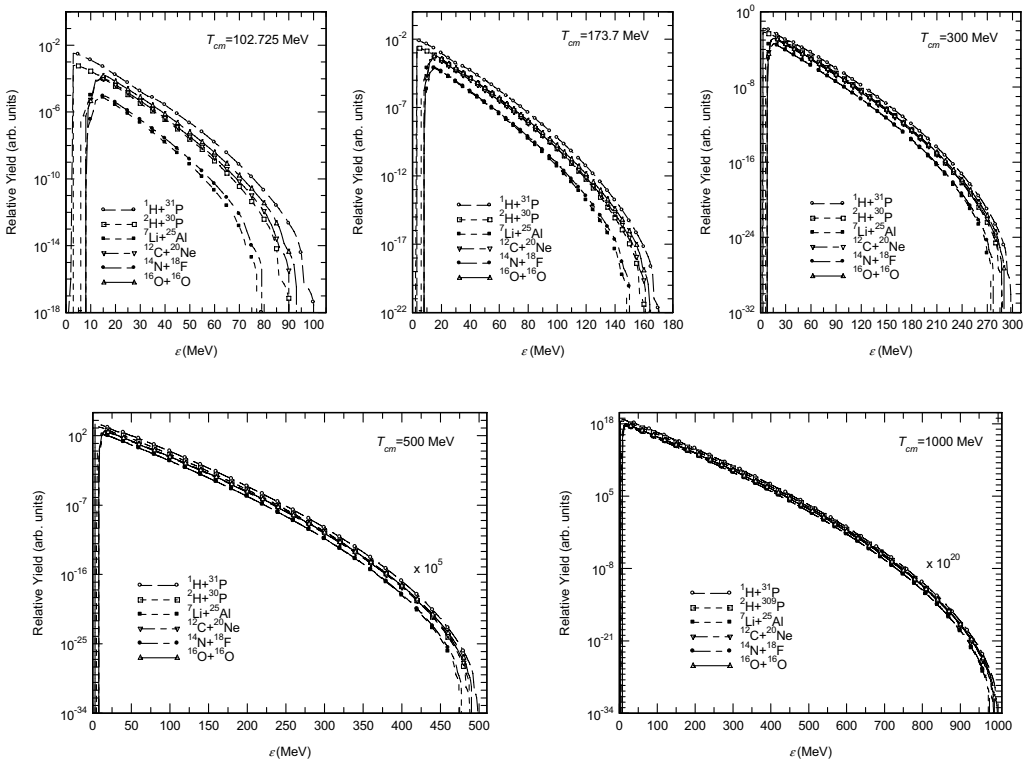

Fig. 1. Relative yields as a function of the relative kinetic energy, ε, for five different pairs of fragments marked, as shown in the figures, for incident energies of 102.7, 173.7, 300, 500, and 1000 MeV (cm). Spectra for 500 and 1000 MeV have been multiplied by the factors indicated in the figure.

4 Results and discussion

To fulfill the goal of this paper, *i.e.* to provide elemental and/or isobaric distributions of nuclei produced in the fragmentation of ^{28}Si by alpha-particle, one should examine the appropriateness of the model to account for the observed data. For this purpose, one should examine the extent to which the model could provide a reasonable account for the distribution of nuclei produced in the fragmentation in experiments.

4.1 Energy spectra

One may use (4) and (7) to compute the ratio $P_{\alpha'}(I, U_C, \theta, \varepsilon)/\Sigma_{\alpha''} P_{\alpha''}(I, U_C)$ in (1) for a given incident energy. This is termed as *relative yield*. The excitation energy of a CN is shared among the relative energy, ε, of the emerging fragments pair and the excitation energies of each member of the pair. Thus, the relative yield is a function of ε. The relative yield at $\varepsilon = 0$ case represents the fact that the entire available energy is transmitted to the excitation of the emerging fragments pair. The relative yields for the maximum value of ε represent the production probabilities of the emission of fragments pair in their ground states.

In fig. 1, we have plotted these relative yields as a function of ε, for the pairs (^{1}H+^{31}P), (^{2}H+^{30}P), (^{7}Li+^{25}Al), (^{12}C + ^{20}Ne), (^{14}N + ^{18}F), and (^{16}O + ^{16}O) for incident alpha-particle energies of 102.7, 173.7, corresponding to lab energies of 117.4 and 198.5 MeV, respectively, 300, 500, and 1000 MeV (cm). These are typical of the kinetic energy spectra. Each relative yield is for a given isobaric pair and has been obtained by summing over the relative yields for each element of a particular isobar. The characteristic features of these spectra are: a) The isobars are emitted in all possible excited states. b) The probabilities of isobars being emitted in highly excited states are much higher than their being emitted in the ground state. c) Each of these curves has a maximum for a given ε, which represents the most probable relative yield at the most probable relative energy, ε_{prob}. This maximum shifts toward $\varepsilon = 0$ with increasing incident energy. This is because the transmission coefficient, $T_0^{12}(\varepsilon)$, in (4), approaches its limiting value of one with the increase in incident energy. In fact, at $T_0^{12}(\varepsilon) = 1$, the relative yield becomes exponential, which is the signature of evaporation. Thus, the non-exponential shape of the relative yields for the production of isobars 16, 20, and 24, indicated in fig. 2, which will be discussed in the following section, is a consequence of incorporating the final-state interaction in (4). d) Although neutrons, protons, and deuterons are emitted preponderantly, the production of heavier elements competes favorably with them in some cases, particularly at higher incident energies.

4.2 Comparison with the data

Woo *et al.* [4] have measured the production of the isobars $A = 16$, 20, and 24 as a function of their lab kinetic energies, E_{lab}, at 30° formed in the ^{4}He + ^{28}Si reaction at

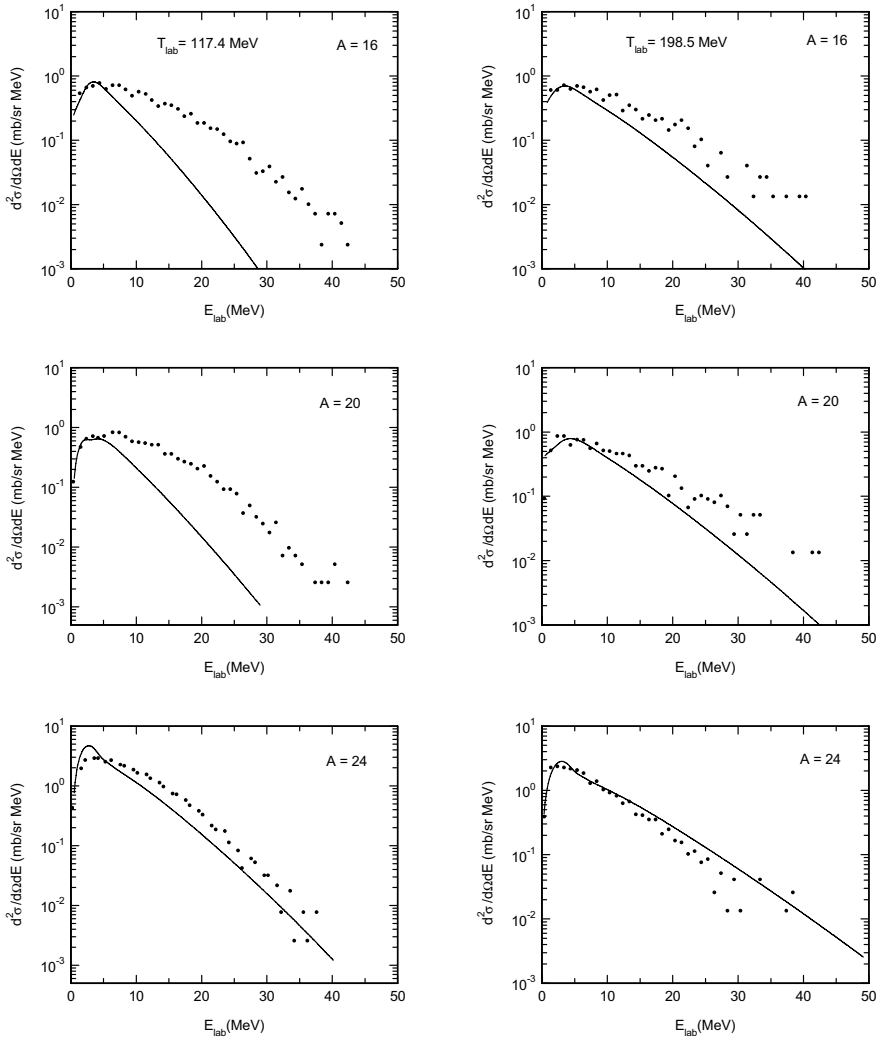

Fig. 2. Kinetic energy spectra at 30° for different fragment mass numbers, as indicated in the figures, for incident energies of 117.4 MeV (left) and 198.5 MeV (right) (lab). Theoretical calculations and the data of [4] are shown by solid lines and solid circles, respectively.

incident energies of 117.4 and 198.5 MeV (lab), and the same for the isobar $A = 24$, at 10°, 30°, 60°, and 90°. They have also measured the differential cross-section for a range of isobars, and hence it would be interesting to apply the model to examine these data. However, to compute the double differential cross-section using (1), and the differential cross-section using (5), one needs knowledge of the CN formation cross-section, σ_C, which is model dependent. To circumvent this problem, one may, however, examine the extent to which the model can account for the relative yields of $A = 16$, 20, and 24 at 30° as a function of E_{lab} of the emerging isobar and the same for $A = 24$ at different angles. This is achieved by normalizing the theoretical production cross-section in one case, in this case for isobar $A = 16$ near forward angles, and then calculating the relative decay probabilities for each isobar as a function of E_{lab} of the emerging fragment for the two given alpha-particle energies. However, in order to compare with the data, the decay probabilities of all elements having a particular mass number are to be summed over.

The experimental data on double differential cross-sections as a function of the lab kinetic energy, E_{lab}, for fragments having a particular mass number, plotted in fig. 2 as solid dots, bears resemblance to the yield curves plotted in fig. 1, implying that these fragments are emitted in various excited states. However, the non-linear behavior of the data as a function of energy in figs. 2 and 3 rules out pure evaporation for this process. The maximum for each mass number is at non-zero energy which is usually characteristic of the statistical model used herein.

In fig. 2 we have compared the calculated probabilities of the emission of isobars $A = 16$, 20, and 24 with the data, as a function of their lab kinetic energies, E_{lab}, for the two incident energies of 117.4 and 198.5 MeV (lab) at 30°. The calculations are normalized to forward angles for $A = 16$. The parameters used in the level density functions are noted earlier. The calculated yields for all the three isobars reproduced the observed energy dependence, thus, providing reasonable support to the validity of this model in calculating fragmentation probabilities. The total decay

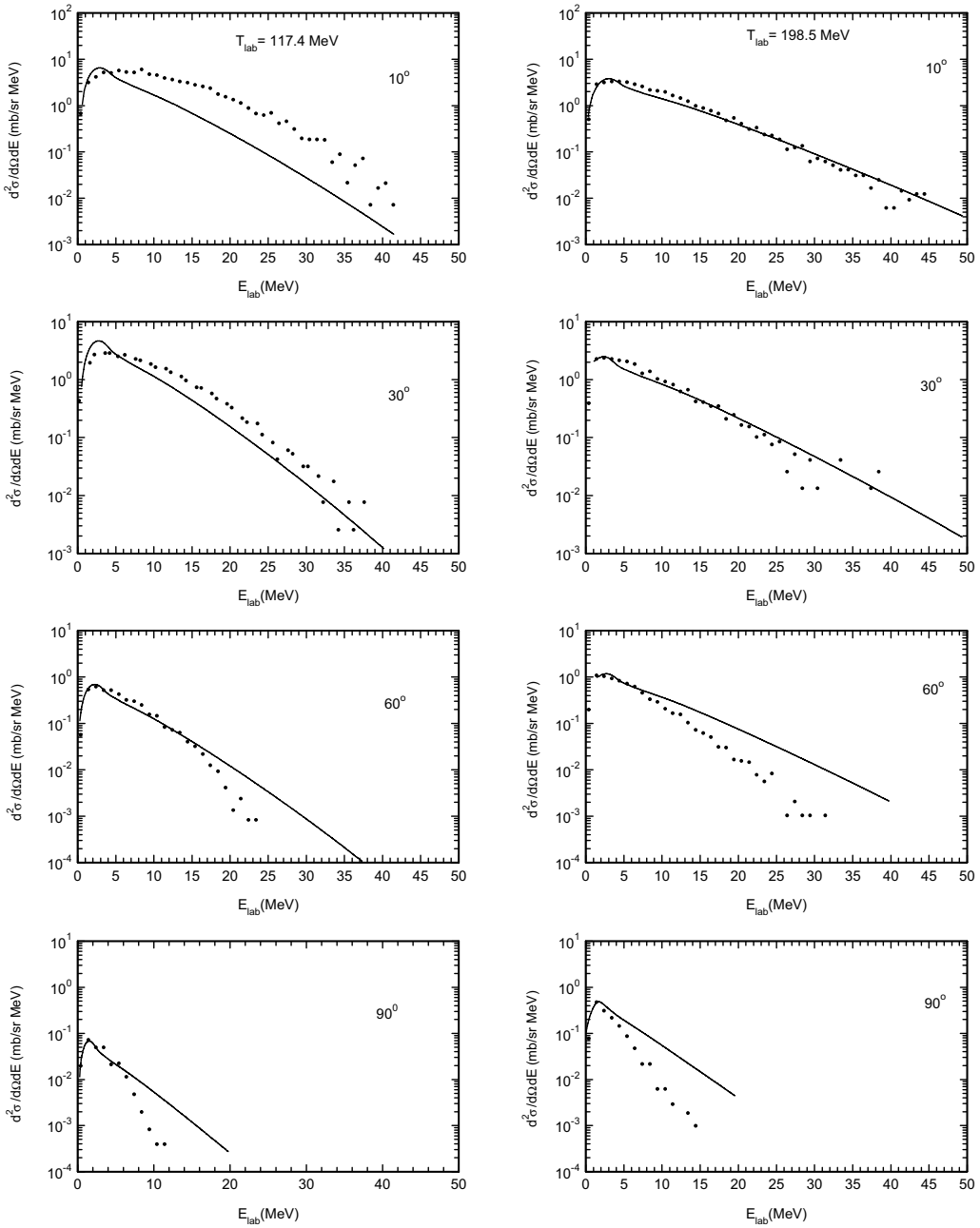

Fig. 3. Kinetic energy spectra for $A = 24$ at different angles, indicated in the figures, for incident energies of 117.4 MeV (left) and 198.5 MeV (right) (lab). Theoretical calculations and the data of [4] are shown by solid lines and solid circles, respectively.

probabilities of a given isobar are obtained by calculating the yields for each element of that isobar and summing over all of them. In our calculations, we have included all the excited elements for the same isobars. It is not clear from the experimental setup whether or not they have been accounted for that.

The double differential cross-sections for the yields of the isobar $A = 24$ have been measured as a function of the lab kinetic energy, E_{lab}, at 10°, 30°, 60°, and 90° for the two incident energies of 117.4 and 198.5 MeV (lab). In fig. 3 the theoretical relative yields as a function of E_{lab} for the production of the isobar $A = 24$ are compared to the data at the two alpha-particle incident energies. Once again, the calculations have been normalized to the data at forward angles. Calculated yields follow the trend of the data at each angle. It is, therefore, reasonable to conclude that the model is suitable in producing the relative yields of elements and isobars.

One may show that the fragments pair in the final channel are emitted in excited states by calculating the excitation energies of the fragments pair, $U_1 + U_2$, using the peaks of the energy spectra. In fig. 4, we have plotted the five theoretical relative yields as a function of the relative energy, ε, for the production of $A = 24$ at the

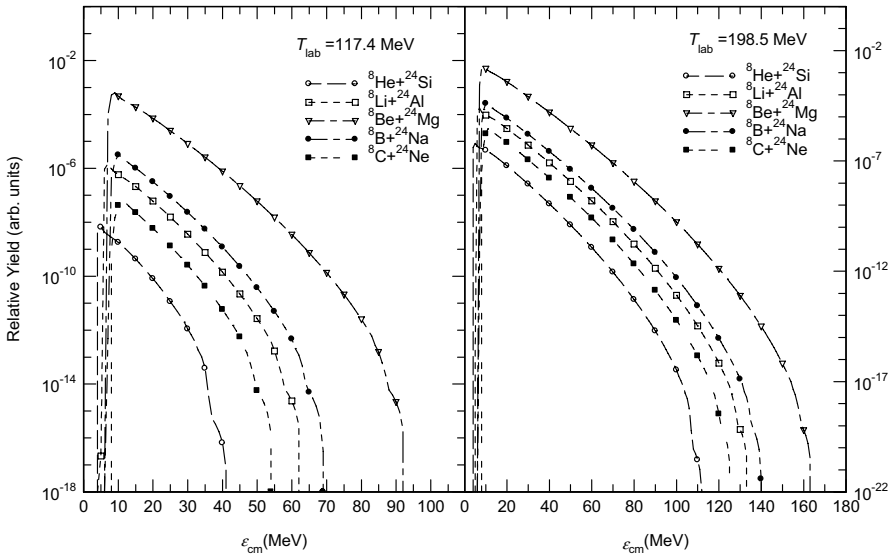

Fig. 4. Relative yields as a function of the relative kinetic energy, ε, for the five elements of the isobar $A = 24$.

Table 1. Excitation energies for $A = 24$.

	$E_{lab} = 117.4$ MeV				$E_{lab} = 198.5$ MeV			
$A_1 + A_2$	ε_{prob} (MeV)	U_H (MeV) calculated	U_H (MeV) measured at 30°	U_H (MeV) measured at 90°	ε_{prob} (MeV)	U_H (MeV) calculated	U_H (MeV) measured at 30°	U_H (MeV) measured at 90°
^{8}He + ^{24}Si	4.5	36.806	39.928	34.414	4.25	108.185	109.759	101.998
^{8}Li + ^{24}Al	6.6	56.168	61.39	55.876	6.6	127.131	131.221	123.46
^{8}Be + ^{24}Mg	8.6	84.049	91.271	85.757	8.65	154.962	161.102	153.341
^{8}B + ^{24}Na	10.1	59.057	67.779	62.265	10.2	129.92	137.61	129.849
^{8}C + ^{24}Ne	11.1	43.414	53.136	47.622	11.3	114.177	122.967	115.206

two incident energies of 117.4 and 198.5 MeV (lab). Each of these curves has a well-defined maximum corresponding to the most probable relative energy, ε_{prob}, indicated in table 1. Assuming that the lighter fragments, *i.e.* ^{8}He, ^{8}Li, ^{8}Be, ^{8}B and ^{8}C, are emitted in their ground states, we have calculated the excitation energies for the heavier fragment, U_H, for the five elements of $A = 24$, as indicated in table 1.

One may compare the calculated results with the measured ones. Woo *et al.* [4] have measured the energy spectra for $A = 24$ at different angles for the two incident energies, as shown in fig. 3. At 30°, the curves peak at $E_{lab} = 4.0$, and 2.5 MeV for 117.4 and 198.5 MeV (lab), respectively. At 90°, both curves peak at $E_{lab} = 1.5$ MeV for 117.4 and 198.5 MeV (lab). Assuming that the heavier fragment $A = 24$ is emitted in an excited state at both energies, we have calculated the excitation energies, U_H, for the five elements of the isobar $A = 24$, as indicated in table 1. The calculated excitation energies are in relatively good agreement with those calculated using the experimental data.

In the case where the two fragments are emitted in excited states, we have calculated the excitation energies for the isobar $A = 16$. In this case, both fragments are emitted in excited states, sharing the total excitation energy equally (since they have the same mass number). For $A = 16$, there are three elements, as indicated in table 2. From their relative yields curves at the two incident energies of 117.4 and 198.5 MeV (lab), we have calculated the most probable relative energy, ε_{prob}, and the total excitation energy, U_T, for the three elements, as indicated in table 2. The total excitation energy, U_T, is the sum of U_1 and U_2. Woo *et al.* [4] have measured the energy spectra for $A = 16$ at 30° for both energies, as shown in fig. 2. Both curves peak at $E_{lab} = 4.5$ and 3.5 MeV for 117.4 and 198.5 MeV (lab), respectively. We have calculated the total excitation energy, U_T, at 30° for the three elements of the isobar $A = 16$, as indicated in table 2. If we assume that the measured excitation energy, U_T, represents the total excitation energy of the pair of fragments for each element, *i.e.* the observed $A = 16$ is for both fragments with $A = 16$, the total calculated and the total measured excitation energies are in relatively good agreement. These results support the interpretation in which the fragments produced in these reactions originate from binary breakup.

Based on the presumption that the pair of fragments are emitted in excited states, the reactions are inelastic, and the data on angular distributions need to be treated as an inelastic process.

Woo *et al.* [4] have measured the differential cross-sections as a function of lab angles, θ_{lab}, for the isobars

Table 2. Excitation energies for $A = 16$.

	$E_{lab} = 117.4$ MeV			$E_{lab} = 198.5$ MeV		
$A_1 + A_2$	ε_{prob} (MeV)	U_T (MeV) calculated	U_T (MeV) measured at 30°	ε_{prob} (MeV)	U_T (MeV) calculated	U_T (MeV) measured at 30°
$^{16}C + ^{16}Ne$	11.0	34.975	42.205	11.0	102.938	107.952
$^{16}N + ^{16}F$	12.0	55.295	63.525	12.0	126.258	129.272
$^{16}O + ^{16}O$	12.0	81.135	89.368	12.0	152.098	155.112

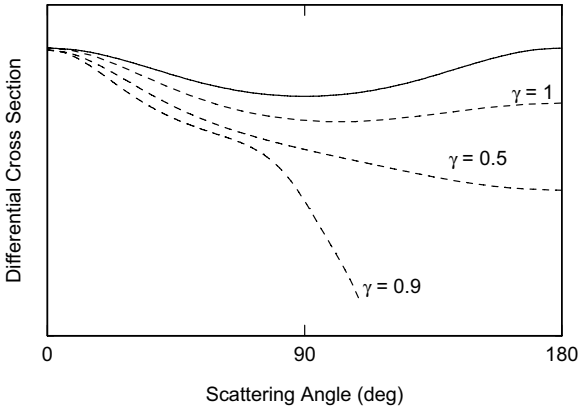

Fig. 5. Typical angular distributions for compound-nucleus reactions induced by light fragments with moderate incident energy. The solid line represents the angular distribution in the cm system, and the dashed line represents the same angular distribution but in the lab system for three different γ values indicated in the figure.

$A = 7$, 12, 16, 20, 24 and 28. In order to account for these data, one needs to use (5) in the lab system. The relation between the differential cross-section in the lab system and the differential cross-section in the cm system is given by

$$\left(\frac{\mathrm{d}\sigma}{\mathrm{d}\Omega}\right)_{lab} = \frac{\left(1+\gamma^2+2\gamma\cos\theta_{cm}\right)^{3/2}}{|1+\gamma\cos\theta_{cm}|}\left(\frac{\mathrm{d}\sigma}{\mathrm{d}\Omega}\right)_{cm}, \quad (15)$$

where γ is defined as the ratio of the speed of the cm in the lab system to the speed of the emitted particle in the cm system. If the Q-value of an inelastic reaction $m_2(m_1, m_3)m_4$ is Q^*, then γ is given by

$$\gamma = \left(\frac{m_1\, m_3}{m_2\, m_4}\,\frac{T_{cm}}{T_{cm}+Q^*}\right)^{1/2}, \quad (16)$$

where T_{cm} is the cm incident energy. One may notice that for fixed m_1, m_2, m_3, m_4, and T_{cm}, γ in (16) is a function of Q^*, *i.e.* $\gamma = \gamma(Q^*)$. This indicates that different values of γ can be obtained by different Q^* values, which implies different values of excitation energies. As an example, for $Q^* = 0$, $m_1 = m_2$, and $m_3 = m_4$, γ is 1, which represents an elastic reaction.

In fig. 5 we have plotted typical angular distributions for compound-nucleus reactions induced by light fragments with moderate incident energy. The solid line represents the angular distribution in the cm system using (5). It is nearly isotropic, which is a characteristic of compound-nucleus reactions. The other three dashed lines represent the angular distributions for the same solid line but in the lab system using (15), and for three different γ values, $\gamma = 1$, which represents an elastic reaction, and the other two values 0.5 and 0.9, corresponding to two different Q^* values, which represent inelastic reactions.

Figure 6 shows the angular distributions for $A = 7$, 12, 16, 20, 24 and 28 for 117.4 and 198.5 MeV (lab). The dashed lines are the calculated ones and the dots connected with solid lines are the measured ones [4]. The γ value used for each mass number is shown in the figure. The differential cross-section of a given isobar is obtained by calculating the yields for each element of that isobar and summing over all of them.

The calculated angular distributions produce the general trend of the observed ones, indicating that the observed data can be well accounted for assuming that a daughter pair is emitted primarily in an excited state. The general trends of the data are commensurate with the binary fragmentation assumption, although multi-particle or sequential decay cannot be ruled out. But the analysis done herein indicated that binary fragmentation is possible and could be a major contributor to the observed cross-sections.

4.3 Elemental, isotopic and isobaric branching ratios

One may use (7) to compute the total decay probability for a given element and, hence, compute the ratio $P_{\alpha'}(I, U_C,)/\Sigma_{\alpha^-} P_{\alpha^-}(I, U_C)$. This ratio is termed as elemental, isotopic, or isobaric branching ratio for the production of elements, or isotopes, or isobars, respectively.

One can construct isotopic branching ratios for each element from hydrogen to ^{31}P from table 3 at incident energies of 102.7, 173.7, 300, 500, and 1000 MeV (cm). In fig. 7, we present these isotopic branching ratios. The most dominant fragments are the isotopes of hydrogen and helium and their respective partners sulfur and silicon. The fragmentation probabilities of heavier elements relative to those of hydrogen and helium increase significantly with the increase in incident energy. These heavy elements are, also, predominantly emitted in excited states.

It is of interest to examine the elemental and isotopic branching ratios for the production of some of the elements of astrophysical interest, particularly, in understanding cosmic abundances. Elements like ^{5}Li and ^{8}Be, which are

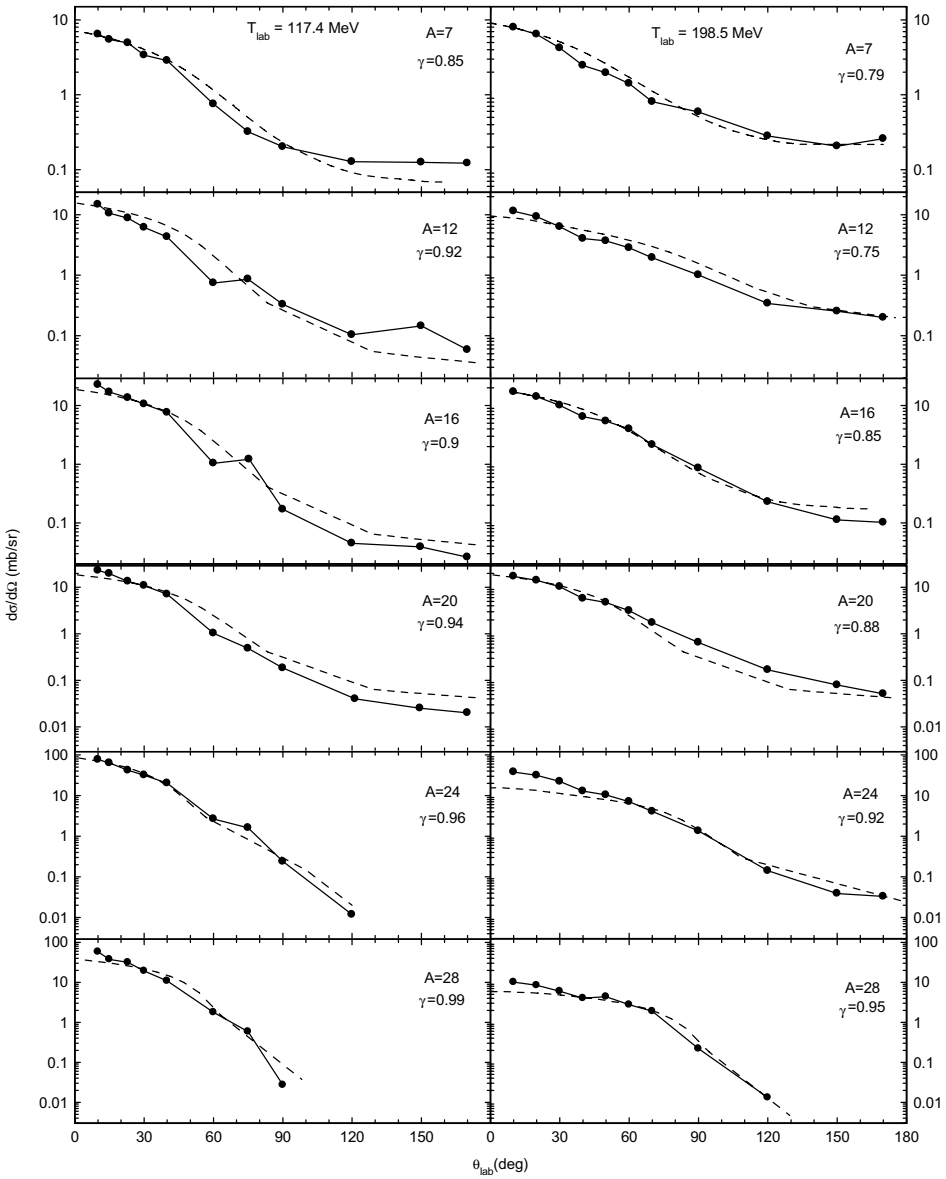

Fig. 6. Angular distributions for several mass numbers, indicated in the figures, for incident energies of 117.4 MeV (left) and 198.5 MeV (right) (lab). Theoretical calculations and the data of [4] are shown by dashed lines and solid circles connected with solid lines, respectively.

unstable, are still produced in significant amounts compared to the production of other elements and their relative abundances increase with increase in incident alpha energy. The production of ^{26}Al, which has astrophysical significance, is comparatively large and increase substantially with the incident energy. The dependence of elemental branching ratios on incident energy implies that the production rates of elements in cosmos, *e.g.* in supernovae, may have significant variance depending on the energetic of the process. Moreover, elements other than hydrogen and helium are predominantly produced in their excited states.

One can construct isobaric branching ratios for isobars 1 to 16 at incident energies of 102.7, 173.7, 300, 500, and 1000 MeV (cm), as indicated in table 4. Each isobaric branching ratio is for a given isobaric pair and has been obtained by summing over the elemental branching ratios for each atomic number of a particular isobar.

In fig. 8 we provide isobaric branching ratios for isobars 1 to 16 at incident energies of 102.7, 173.7, 300, 500, and 1000 MeV (cm). The production of the corresponding isobaric partners of $A = 16$ to 31 can be deduced from this figure by looking at the yields for its complementary partner, for example, the yields for $A = 17$ are the same as those of its partner, $A = 15$. As expected, at lower incident energies, the maximum yields are those of $A = 1$, 2, 3, and 4. But the comparative yields of heavier isobars increase with increasing incident energy. At 1.0 GeV incident energy yields of $A = 16$ to 27 (or corresponding partner 16 to 5) are comparable to those of $A = 1$ to 4. *Most importantly, all isotopes are emitted predominantly in excited states.* This possibility, which is a major out-

Table 3. Isotopic branching ratios for each atomic number for five energies.

A_1	A_2	Z_1	Z_2	Final channel	Isotopic branching ratio				
					102.7 MeV	173.7 MeV	300 MeV	500 MeV	1000 MeV
n	S	0	16	1n0 + 31S16	4.99E-02	9.15E-02	9.83E-02	1.00E-01	9.11E-02
H	P	1	15	1H1 + 31P15	1.99E-01	1.62E-01	2.56E-01	2.09E-01	1.44E-01
				2H1 + 30P15	4.47E-02	5.49E-02	9.67E-02	9.25E-02	7.08E-02
				3H1 + 29P15	2.41E-02	3.03E-02	7.74E-02	6.53E-02	4.45E-02
				4H1 + 28P15	2.08E-04	1.15E-03	3.43E-03	7.43E-03	9.94E-03
He	Si	2	14	3He2 + 29Si14	3.29E-02	5.23E-02	4.02E-02	5.95E-02	4.94E-02
				4He2 + 28Si14	5.02E-01	2.93E-01	1.45E-01	2.06E-01	8.87E-02
				5He2 + 27Si14	1.11E-02	2.18E-02	1.94E-02	3.09E-02	3.09E-02
				6He2 + 26Si14	8.80E-04	3.42E-03	4.31E-03	1.08E-02	1.15E-02
				7He2 + 25Si14	5.87E-06	1.33E-04	4.07E-04	2.18E-03	3.09E-03
				8He2 + 24Si14	2.29E-07	1.44E-05	8.51E-05	5.10E-04	1.33E-03
Li	Al	3	13	4Li3 + 28Al13	6.98E-04	5.18E-03	6.52E-03	8.09E-03	1.55E-02
				5Li3 + 27Al13	5.27E-02	3.99E-02	3.24E-02	7.16E-02	3.99E-02
				6Li3 + 26Al13	3.13E-03	1.30E-02	1.15E-02	1.19E-02	2.03E-02
				7Li3 + 25Al13	1.17E-03	6.63E-03	6.68E-03	8.22E-03	1.41E-02
				8Li3 + 24Al13	4.72E-05	5.62E-04	1.12E-03	3.12E-03	5.18E-03
				9Li3 + 23Al13	3.49E-06	8.34E-05	2.94E-04	1.75E-03	2.53E-03
				10Li3 + 22Al13	5.64E-09	1.94E-06	2.40E-05	1.10E-04	6.67E-04
Be	Mg	4	12	6Be4 + 26Mg12	1.94E-03	5.73E-03	1.07E-02	6.50E-03	1.40E-02
				7Be4 + 25Mg12	2.37E-03	1.17E-02	9.83E-03	5.73E-03	1.80E-02
				8Be4 + 24Mg12	2.08E-02	5.93E-02	3.40E-02	1.47E-02	3.39E-02
				9Be4 + 23Mg12	1.14E-03	5.62E-03	6.04E-03	3.78E-03	1.28E-02
				10Be4 + 22Mg12	2.53E-06	6.27E-05	2.57E-04	3.44E-04	2.31E-03
				11Be4 + 21Mg12	3.34E-06	7.12E-05	2.95E-04	3.75E-04	2.49E-03
				12Be4 + 20Mg12	8.42E-08	7.15E-06	7.11E-05	1.29E-04	1.15E-03
B	Na	5	11	7B5 + 25Na11	7.11E-05	4.61E-04	1.56E-03	1.42E-03	6.73E-03
				8B5 + 24Na11	2.20E-04	1.42E-03	2.34E-03	1.88E-03	7.92E-03
				9B5 + 23Na11	2.04E-03	1.03E-02	8.51E-03	4.92E-03	1.51E-02
				10B5 + 22Na11	9.03E-04	4.43E-03	5.18E-03	3.33E-03	1.14E-02
				11B5 + 21Na11	9.93E-04	4.22E-03	5.23E-03	3.30E-03	1.18E-02
				12B5 + 20Na11	4.78E-05	3.70E-04	1.04E-03	9.65E-04	4.92E-03
				13B5 + 19Na11	3.52E-06	5.93E-05	3.42E-04	4.15E-04	2.69E-03
				14B5 + 18Na11	1.23E-08	1.09E-06	3.15E-05	7.03E-05	7.56E-04
C	Ne	6	10	8C6 + 24Ne10	2.20E-06	3.99E-05	4.14E-04	5.15E-04	3.33E-03
				9C6 + 23Ne10	1.94E-05	1.19E-04	7.55E-04	7.85E-04	4.08E-03
				10C6 + 22Ne10	7.33E-04	5.05E-03	4.73E-03	3.09E-03	1.05E-02
				11C6 + 21Ne10	1.31E-03	5.26E-03	6.26E-03	3.81E-03	1.24E-02
				12C6 + 20Ne10	1.35E-02	3.32E-02	2.34E-02	1.04E-02	2.71E-02
				13C6 + 19Ne10	1.37E-03	4.48E-03	6.01E-03	3.62E-03	1.29E-02
				14C6 + 18Ne10	6.86E-04	2.43E-03	3.99E-03	2.64E-03	1.03E-02
				15C6 + 17Ne10	6.21E-06	7.25E-05	4.87E-04	5.36E-04	3.27E-03
				16C6 + 16Ne10	2.31E-07	7.54E-06	1.25E-04	1.93E-04	1.58E-03
N	F	7	9	10N7 + 22F9	6.66E-08	3.47E-06	7.60E-05	1.39E-04	1.11E-03
				11N7 + 21F9	1.68E-05	8.71E-05	6.21E-04	6.55E-04	3.30E-03
				12N7 + 20F9	7.41E-05	6.32E-04	1.46E-03	1.24E-03	5.49E-03
				13N7 + 19F9	1.65E-03	4.53E-03	6.74E-03	3.96E-03	1.35E-02
				14N7 + 18F9	1.71E-03	4.51E-03	6.75E-03	3.96E-03	1.37E-02
				15N7 + 17F9	2.37E-03	6.19E-03	8.13E-03	4.55E-03	1.52E-02
				16N7 + 16F9	9.85E-05	4.07E-04	1.56E-03	1.29E-03	6.13E-03
O	O	8	8	12O8 + 20O8	3.48E-07	9.82E-06	1.63E-04	2.39E-04	1.60E-03
				13O8 + 19O8	6.58E-06	6.92E-05	4.91E-04	5.44E-04	3.08E-03
				14O8 + 18O8	8.20E-04	2.23E-03	4.53E-03	2.91E-03	1.09E-02
				15O8 + 17O8	2.37E-03	5.70E-03	8.13E-03	4.55E-03	1.52E-02
				16O8 + 16O8	2.02E-02	4.53E-02	2.95E-02	1.23E-02	3.14E-02
F	N	9	7	14F9 + 18N7	1.62E-08	1.59E-06	4.19E-05	8.62E-05	8.57E-04
				15F9 + 17N7	8.50E-06	8.83E-05	5.94E-04	6.24E-04	3.62E-03
Total					1	1	1	1	1

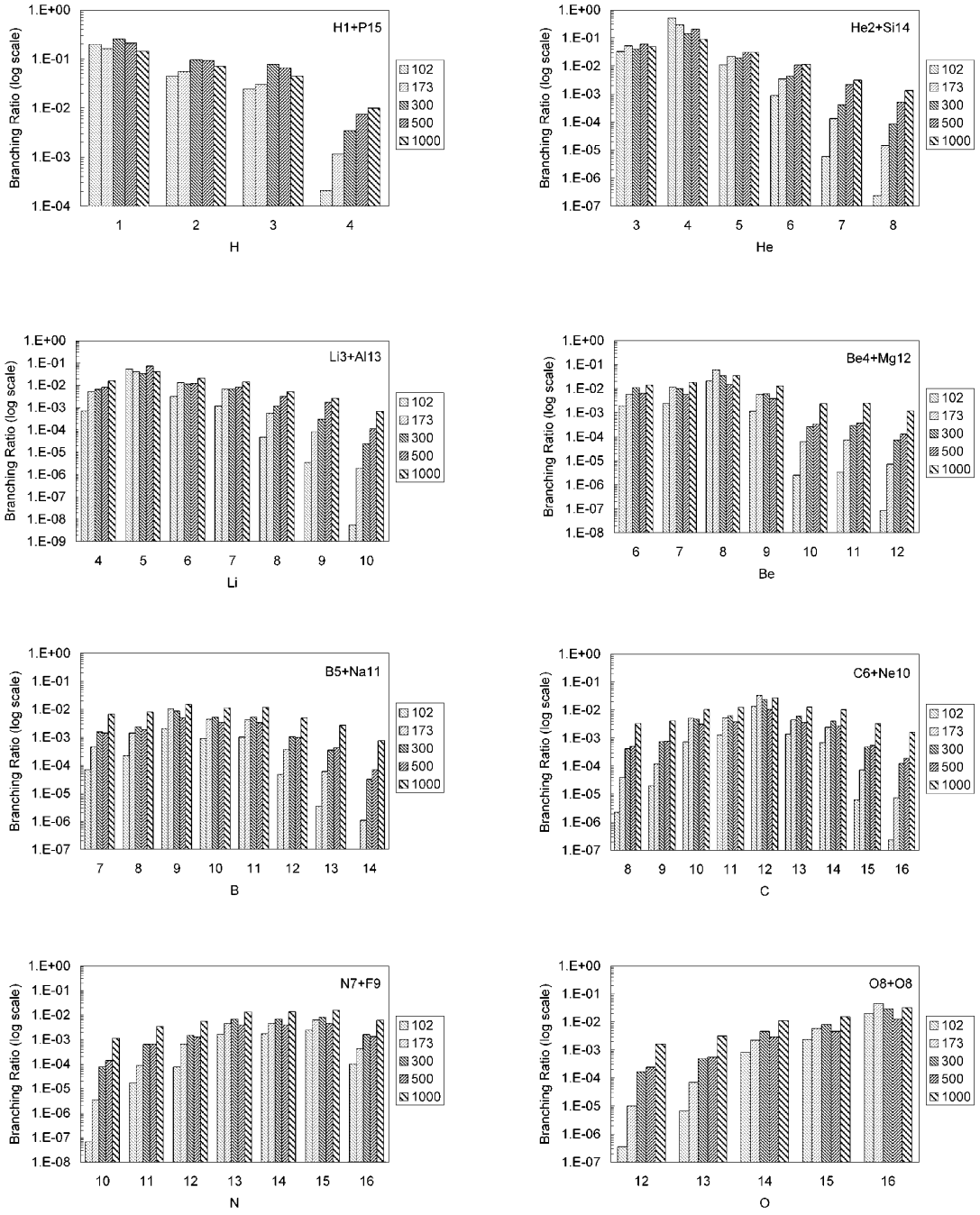

Fig. 7. Isotopic branching ratios for the final channels in table 3 as a function of the mass number of A_1 for incident energies of 102.7, 173.7, 300, 500, and 1000 MeV (cm). The productions of the corresponding partner A_2 are the same of A_1.

come of this model, has been quite often overlooked in many previous calculations.

An interesting feature of fig. 8 is that the relative yields of lighter mass and heavier mass nuclei actually go up with increasing incident energy of the projectile. In the simplest version of the evaporation model, one expects this to go down with energy. But in the model discussed here this occurs because of the incorporation of the final-state interaction, because at higher energies, the decay probability is determined by competition between three exponential functions of energy as discussed in [21]. The situation is similar to the observed increase of the ratio of light to heavy fragment with increasing neutron energy in neutron-induced fission which is well accountable for by a theory similar to the one used in [21].

The branching ratios provided in table 4 reflect the relative production rates. The computation of absolute production rates involves calculations of the CN formation cross-section, σ_C, for which there is no standard method. The reasonable accurate method of Haider and Malik [17]

Table 4. Total isobaric branching ratios for each isobaric pair for five energies.

A_1	A_2	Final channel	Total isobaric branching ratio				
			102.7 MeV	173.7 MeV	300 MeV	500 MeV	1000 MeV
1	31	1n0 + 31S16 1H1 + 31P15	0.2485	0.2536	0.3544	0.3092	0.2351
2	30	2H1 + 30P15	0.0447	0.0549	0.0967	0.0925	0.0708
3	29	3H1 + 29P15 3He2 + 29Si14	0.0570	0.0826	0.1176	0.1247	0.0939
4	28	4H1 + 28P15 4He2 + 28Si14 4Li3 + 28Al13	0.5034	0.2991	0.1547	0.2219	0.1141
5	27	5He2 + 27Si14 5Li3 + 27Al13	0.0638	0.0617	0.0519	0.1025	0.0708
6	26	6He2 + 26Si14 6Li3 + 26Al13 6Be4 + 26Mg12	0.0059	0.0221	0.0264	0.0293	0.0458
7	25	7He2 + 25Si14 7Li3 + 25Al13 7Be4 + 25Mg12 7B5 + 25Na11	0.0036	0.0189	0.0185	0.0176	0.0420
8	24	8He2 + 24Si14 8Li3 + 24Al13 8Be4 + 24Mg12 8B5 + 24Na11 8C6 + 24Ne10	0.0210	0.0614	0.0379	0.0207	0.0517
9	23	9Li3 + 23Al13 9Be4 + 23Mg12 9B5 + 23Na11 9C6 + 23Ne10	0.0032	0.0161	0.0156	0.0112	0.0345
10	22	10Li3 + 22Al13 10Be4 + 22Mg12 10B5 + 22Na11 10C6 + 22Ne10 10N7 + 22F9	0.0016	0.0096	0.0103	0.0070	0.0260
11	21	11Be4 + 21Mg12 11B5 + 21Na11 11C6 + 21Ne10 11N7 + 21F9	0.0023	0.0096	0.0124	0.0081	0.0300
12	20	12Be4 + 20Mg12 12B5 + 20Na11 12C6 + 20Ne10 12N7 + 20F9 12O8 + 20O8	0.0136	0.0342	0.0262	0.0130	0.0403
13	19	13B5 + 19Na11 13C6 + 19Ne10 13N7 + 19F9 13O8 + 19O8	0.0030	0.0091	0.0136	0.0085	0.0321
14	18	14B5 + 18Na11 14C6 + 18Ne10 14N7 + 18F9 14O8 + 18O8 14F9 + 18N7	0.0032	0.0092	0.0153	0.0097	0.0365
15	17	15C6 + 17Ne10 15N7 + 17F9 15O8 + 17O8 15F9 + 17N7	0.0048	0.0121	0.0173	0.0103	0.0373
16	16	16C6 + 16Ne10 16N7 + 16F9 16O8 + 16O8	0.0203	0.0458	0.0312	0.0138	0.0391
TOTAL			1	1	1	1	1

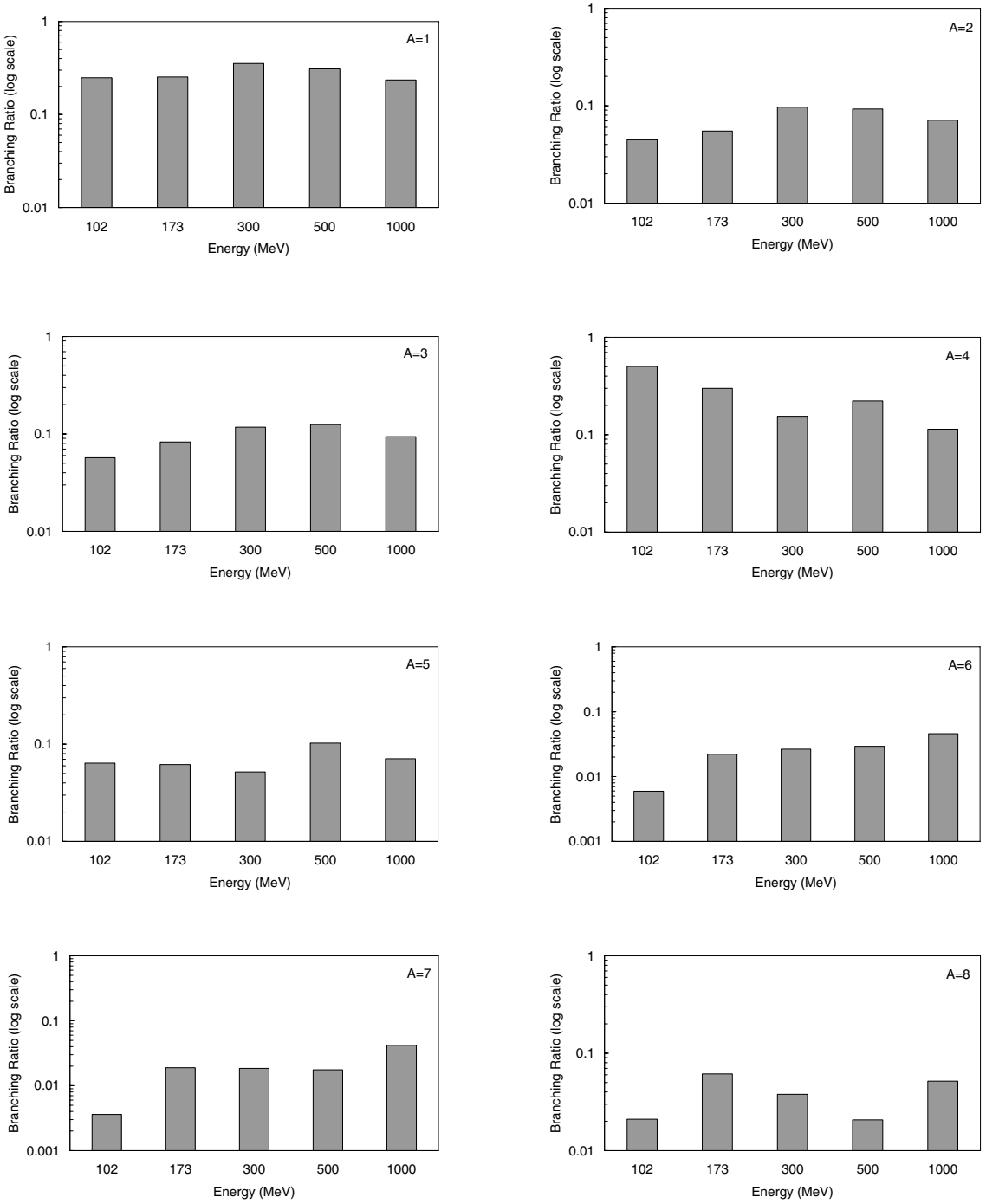

Fig. 8. Isobaric branching ratios for the isobars $A = 1$ to 16 as a function of the cm incident energies. The production of the corresponding isobaric partners of $A = 16$ to 31 can be deduced from this figure by looking at the yields for its complementary partner, *i.e.* the yields for $A = 20$ are the same as those of its partner $A = 12$.

to compute capture cross-section of two colliding heavy ions has not been tested for alpha-particle capture and depends on the details of the potential of two colliding ions. In addition to these methods, there are a number of simple global methods employed to estimate the compound-nucleus formation cross-sections described in refs. [5,22–27]. The absolute production cross-section of a particular element, or its isotopes can be obtained by simply multiplying its branching ratio, noted in table 4 by the CN formation cross-sections, σ_C, at all energies.

Woo *et al.* [4] have measured the total reaction cross-sections for the two energies 117.4 and 198.5 MeV (lab) by summing up the $A \geq 6$ cross-sections directly, but the production cross-section of $A = 1$, 2, 3, 4 and 5 are not included in their measurements. However, we note that theoretically the production cross-section for $A = 1$, 2, 3,

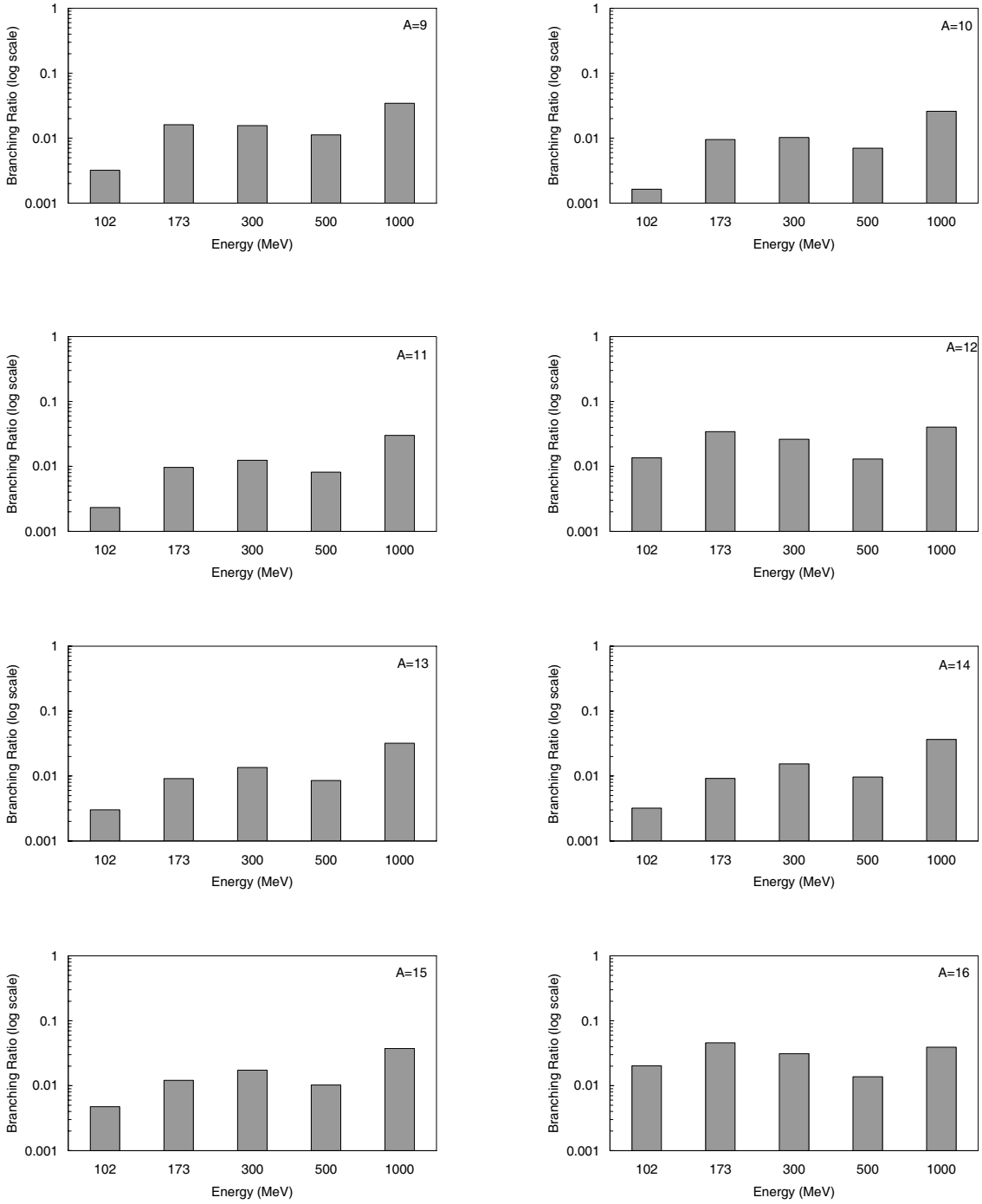

Fig. 8. Continued.

Table 5. Total reaction cross-sections (mb).

E_{cm} (MeV)	σ_R[a]	σ_R[b]	σ_R[c]	σ_R[d]	σ_R (this work)
102.7	670	950	1212	1230	1483
173.7	640	950	1133	1104	1366
300.0	–	–	–	–	1232
500.0	–	–	–	–	1100
1000.0	–	–	–	–	927

[a] Reference [4]; [b] ref. [28]; [c] ref. [29]; [d] ref. [30].

4, and 5 is significant. As such, the measured cross-section represents the lower limit of the cross-section, and the actual cross-section should be significantly higher. Our calculations for the total cross-section for these two energies are listed in table 5 and compared with the data of [4] and the predicted calculations from Webber *et al.* [28], Kox *et al.* [29], and Karol [30]. We have also calculated the total cross-section for energies 300, 500, and 1000 MeV (cm) as indicated in table 5. Our calculations are in relatively

good agreement with the other calculations [28–30] and indicate the expected decrease in the reaction cross-section with increasing energy due to the target transparency.

5 Conclusion

The calculations of fragmentation cross-sections in this paper indicate that nuclei in alpha-induced fragmentation of ^{28}Si are emitted in all possible excited and ground states allowed by the energy conservation. In fact, the probabilities of fragments being emitted in excited states are significantly higher than those being emitted in ground states, except for hydrogen and helium, at all incident energies. While H and He are dominant fragments at all incident energies, as expected, the relative production rate of these two elements compared to those of other elements reduces significantly with increasing incident energies. The theory can reproduce the observed energy dependence of isobars 16, 20, and 24 at 30° and the isobar 24, at a few other angles. In addition, the observed angular distributions of the production cross-sections for $A = 7$, 12, 16, 20, and 28 are well accounted for, assuming the emitted fragments to be in excited states. Obviously, direct processes are likely to contribute additionally to the production of light elements, particularly, isotopes of hydrogen and helium at forward angles. However, the production of other elements is expected to be reasonably described by this model.

The authors are pleased to acknowledge the NSF grant No. INT-0209583. The authors thank Dr. Ram Tripathi for discussion.

References

1. J.W. Wilson, L.W. Townsend, W. Schimmerling, G.S. Khandelwal, F. Khan, J.E. Nealy, F.A. Cucinotta, L.C. Simonsen, J.L. Shinn, J.W. Norbury, *Transport Methods and Interactions for Space Radiations*, NASA Ref. Publication No. 1257 (1991).
2. L.H. Ahrens, *Origin and Distribution of the Elements* (Pergamon Press, Oxford, 1968).
3. B. Compani-Tabrizi, F.B. Malik, J. Phys. G **8**, 1447 (1982).
4. L.W. Woo, K. Kwiatkowski, W.G. Wilson, V.E. Viola, Phys. Rev. C **47**, 267 (1993).
5. V.F. Weisskopf, D.H. Ewing, Phys. Rev. **57**, 472 (1940).
6. T.D. Newton, *Proceedings of the Symposium on the Physics of Fission (1956) Chalk Revier*, Report CRO-642-A: Report AECL-329.
7. T. Ericson, Adv. Phys. **9**, 425 (1960).
8. E. Gadioli, L. Zetta, Phys. Rev. **167**, 1016 (1968).
9. A.G.W. Cameron, Can. J. Phys. **36**, 1040 (1958).
10. B. Block, J.W. Clark, M.D. High, R. Malmin, F.B. Malik, Ann. Phys. (N.Y.) **62**, 464 (1971).
11. I. Reichstein, F.B. Malik, Ann. Phys. (N.Y.) **98**, 322 (1976).
12. I. Reichstein, F.B. Malik, *Super-Heavy Elements*, edited by M.A.K. Lodhi (Gordon and Breach, 1978).
13. F.B. Malik, I. Reichstein, *Clustering Phenomena in Atoms and Nuclei*, edited by M.A. Brenner, T. Lonnroth, F.B. Malik (Springer Verlag, 1992).
14. W. Scheid, R. Ligensa, W. Greiner, Phys. Rev. Lett. **21**, 1479 (1968).
15. M.A. Alam, F.B. Malik, *Clustering Phenomena in Atoms and Nuclei*, edited by M.A. Brenner, T. Lonnroth, F.B. Malik (Springer Verlag, 1992).
16. L. Rickertsen, B. Block, J. Clark, F.B. Malik, Phys. Rev. Lett. **22**, 951 (1969).
17. Q. Haider, F.B. Malik, J. Phys. G **7**, 1661 (1981).
18. P. Manngard, M. Brenner, M. Alam, I. Reichstein, F.B. Malik, Nucl. Phys. A **504**, 130 (1989).
19. P. Manngard, M. Brenner, I. Reichstein, F.B. Malik, *Proceedings of the 5th International Conference on Nuclear Reaction Mechanisms*, edited by E. Gadioli (University of Milano Press, 1989).
20. Z.F. Shehadeh, PhD Dissertation, Southern Illinois University at Carbondale (1994).
21. M.A. Hooshyar, I. Reichstein, F.B. Malik, *Nuclear Fission and Cluster Radioactivity* (Spring-Verlag, 2005) Chapt. 6.
22. J.M. Blatt, V.F. Weisskopf, *Theoretical Nuclear Physics* (John Wiley and Sons, New York, 1952).
23. R.K. Tripathi, F.A. Cucinotta, J.W. Wilson, Nucl. Instrum. Methods B **155**, 349 (1999).
24. R.K. Tripathi, F.A. Cucinotta, J.W. Wilson, NASA TP, 209726 (1999).
25. R.K. Tripathi, J.W. Wilson, F.A. Cucinotta, Nucl. Instrum. Methods B **129**, 11 (1997).
26. R.K. Tripathi, F.A. Cucinotta, J.W. Wilson, NASA TP, 3621 (1997).
27. R.K. Tripathi, F.A. Cucinotta, J.W. Wilson, Nucl. Instrum. Methods B **117**, 347 (1996).
28. W.R Webber, J.C. Kish, D.A. Schrier, Phys. Rev. C **41**, 520 (1990).
29. S. Kox, A. Gamp, R. Cherkaoui, A.J. Cole, N. Longequeue, J. Menet, C. Perrin, J. Viano, Nucl. Phys. A **420**, 162 (1984).
30. P.J. Karol, Phys. Rev. C **11**, 1203 (1975).